Isolation of a Stable Precursor for [Pt^0(P−P)] and Its Reductive Addition to $Ru_3(CO)_9(\mu_3\text{-}S)_2$ Giving Square Heterometallic Clusters Supported by Two Face-Capping μ_4-Sulfides [P−P = $(C_5H_4PPh_2)_2M$; M = Fe, Ru]

S.-W. Audi Fong, Jagadese J. Vittal, and T. S. Andy Hor*,†

Department of Chemistry, Faculty of Science, National University of Singapore, 3 Science Drive 3, Singapore 117543

Received July 20, 1999

Two labile but air-stable Pt(0) complexes Pt(η^2-P−P)(η^2-dba) [dba = dibenzylideneacetone; P−P = 1,1′-bis(diphenylphosphino)ferrocene (dppf) (**3a**) or 1,1′-bis(diphenylphosphino)-ruthenocene (dppr) (**3b**)] were prepared from $Pt_2(dba)_3$ (**1**) and the corresponding metallocenyl diphosphine. Reductive addition of **3** to $Ru_3(CO)_9(\mu_3\text{-}S)_2$ (**4**) gave good yields of two novel square clusters $PtRu_3(CO)_6(\mu\text{-}CO)_2(\eta^2\text{-}P{-}P)(\mu_4\text{-}S)_2$ [P−P = dppf (**5a**) or dppr (**5b**)]. A one-pot reaction mixture containing **1**, **4**, and the diphosphine (**2**) gave $Ru_3(CO)_7(\mu\text{-}P{-}P)(\mu_3\text{-}S)_2$ [P−P = dppf (**6a**) or dppr (**6b**)] along with **5a** and **5b**. All products have been characterized by IR, ^1H, and $^{31}P\{^1H\}$ NMR. In addition, X-ray crystal analyses were also performed on complexes **3a**, **5a**, **5b**, and **6a**. **3a** is a planar Pt(0)−olefin complex stabilized by chelating dppf and a *trans,trans*-dba moiety coordinated via a C=C functionality. Compounds **5a** and **5b** are rare examples of almost regularly octahedral heterometallic square clusters with two μ_4-S ligands above and below the $PtRu_3$ plane.

Introduction

Bis(phosphine)platinum−olefin complexes are valuable precursors in an array of inorganic syntheses.[1] Adams et al., for example, had adopted this reductive addition approach for the synthesis of heterometallic clusters whereby a low-valent metal fragment like [Pt-$(PPh_3)_2$]^2 is introduced to a cluster core, such as $M_3(CO)_9(\mu_3\text{-}S)_2$ (M = Os, Ru).[3] This is a powerful strategy in cluster expansion reactions, although the product mixture is often complicated by secondary reactions arising from phosphine dissociation, migration, and exchanges with the carbonyls on the cluster core. The ease of M−M and M−S bond formation and cleavage also leads to a variety of fascinating but unpredictable cluster structures. Our interest in the metallocenyl diphosphines (P−P) such as dppf[4] (**2a**) [dppf = 1,1′-bis-(diphenylphosphino)ferrocene] and dppr[5] (**2b**) [dppr = 1,1′-bis(diphenylphosphino)ruthenocene] stems from their rich catalytic and electroactive potential. This approach would provide a simple entry into electroactive clusters if a precursor like Pt(η^2-P−P)(η^2-C_2H_4) can be synthesized and isolated easily. Such a precursor would be a direct source for the unsaturated [Pt(P−P)] species, which is synthetically and catalytically powerful,[6] especially if it can be easily synthesized and is stable enough to be kept and handled in air. Our numerous attempts to isolate such a complex have been unsuccessful. Prompted by strong current interest in dba complexes of palladium in organometallic syntheses[7] and catalysis,[8] we turned our attention to the synthesis of the dba analogues, viz. Pt(η^2-P−P)(η^2-dba) [P−P = dppf (**3a**) or dppr (**3b**); dba = dibenzylideneacetone or *E,E*-1,5-diphenyl-1,4-pentadien-3-one]. Their usefulness

† Fax: 65-7791691. E-mail: chmandyh@nus.edu.sg.

(1) (a) Uddin, J.; Dapprich, S.; Frenking, G.; Yates, B. F. *Organometallics* **1999**, *18*, 457. (b) Nicolaides, A.; Smith, J. M.; Kumar, A.; Barnhart, D. M.; Borden, W. T. *Organometallics* **1995**, *14*, 3475. (c) Kumar, A.; Lichtenhan, J. D.; Critchlow, S. C.; Eichinger, B. E.; Borden, W. T. *J. Am. Chem. Soc.* **1990**, *112*, 5633.

(2) (a) Cheng, P. T.; Cook C. D.; Nyburg, S. C.; Wan, K. Y. *Inorg. Chem.* **1971**, *10*, 2210. (b) Cheng, P. T.; Nyburg, S. C. *Can. J. Chem.* **1972**, *50*, 912. (c) Head, R. A. *Inorg. Synth.* **1990**, *28*, 132. (d) Hartley, F. R. *The Chemistry of Platinum and Palladium*; Applied Science Publishers: London, 1973; p 398. (e) Berry, M.; Howard, J. A. K.; Stone, F. G. A. *J. Chem. Soc., Dalton Trans.* **1980**, 1601. (f) Nuzzo, R. G.; McCarthy, T. J.; Whitesides, G. M. *Inorg. Chem.* **1981**, *20*, 1312.

(3) (a) Adams, R. D.; Hor, T. S. A.; Horváth, I. T. *Inorg. Chem.* **1984**, *23*, 4733. (b) Adams, R. D.; Lii, J.-C.; Wu, W. *J. Cluster Sci.* **1993**, *4*, 423. (c) Adams, R. D.; Babin, J. E.; Mathab, R.; Wang, S. *Inorg. Chem.* **1986**, *25*, 1623.

(4) (a) Gan, K.-S.; Hor, T. S. A. In *Ferrocenes−Homogeneous Catalysis, Organic Synthesis, Materials Science*; Togni, A., Hayashi, T., Eds.; VCH: Weinheim, FRG, 1995; pp 3−104. (b) Fong, S.-W. A.; Hor, T. S. A. *J. Cluster Sci.* **1998**, *9*, 351. (c) Low, P. M. N.; Tan, A. L.; Hor, T. S. A.; Wen, Y.-S.; Liu, L.-K. *Organometallics* **1996**, *15*, 2595. (d) Yeo, J. S. L.; Li, G.; Yip, W. H.; Henderson, W.; Mak, T. C. W.; Hor, T. S. A. *J. Chem. Soc., Dalton Trans.* **1999**, 435. (e) Jiang, C.; Wen, Y.-S.; Liu, L.-K.; Hor, T. S. A.; Yan, Y. K. *Organometallics* **1998**, *17*, 173.

(5) (a) Yeo, S. P.; Henderson, W.; Mak, T. C. W.; Hor, T. S. A. *J. Organomet. Chem.* **1999**, *575*, 171. (b) Li, S.; Wei, B.; Low, P. M. N.; Lee, H. K.; Hor, T. S. A.; Xue, F.; Mak, T. C. W. *J. Chem. Soc., Dalton Trans.* **1997**, 1289. (c) Wei, B.; Li, S.; Lee, H. K.; Hor, T. S. A. *J. Organomet. Chem.* **1997**, *527*, 133. (d) Wei, B.; Li, S.; Lee, H. K.; Hor, T. S. A. *J. Mol. Catal. A: Chem.* **1997**, *126*, L83. (e) Li, C.; Low, P. M. N.; Li, S.; Lee, H. K.; Hor, T. S. A. *Chromatographia* **1997**, *44*, 381.

(6) (a) Gavagnin, R.; Cataldo, M.; Pinna, F.; Strukul, G. *Organometallics* **1998**, *17*, 661. (b) Strukul, G.; Varagnolo, A.; Pinna, F. *J. Mol. Catal. A: Chem.* **1997**, *117*, 413. (c) Kollar, L.; Kegl, T.; Bakos, J. *J. Organomet. Chem.* **1993**, *453*, 155.

(7) Tsuji, J. *Palladium and Catalysts: Innovations in Organic Synthesis*; Wiley & Sons: New York, 1995; pp 13−18.

(8) (a) Amatore, C.; Jutand, A. *Coord. Chem. Rev.* **1998**, *180*, 511. (b) Burrows, A. D.; Choi, N.; McPartlin, M.; Mingos, D. M. P.; Tarlton, S. V.; Vilar, R. *J. Organomet. Chem.* **1999**, *573*, 313. (c) Oshiki, T.; Mashima, K.; Yamagata, T.; Tani, K. *Bull. Chem. Soc. Jpn.* **1998**, *71*, 2859.

10.1021/om990569c CCC: $19.00
Publication on Web 02/10/2000

Scheme 1

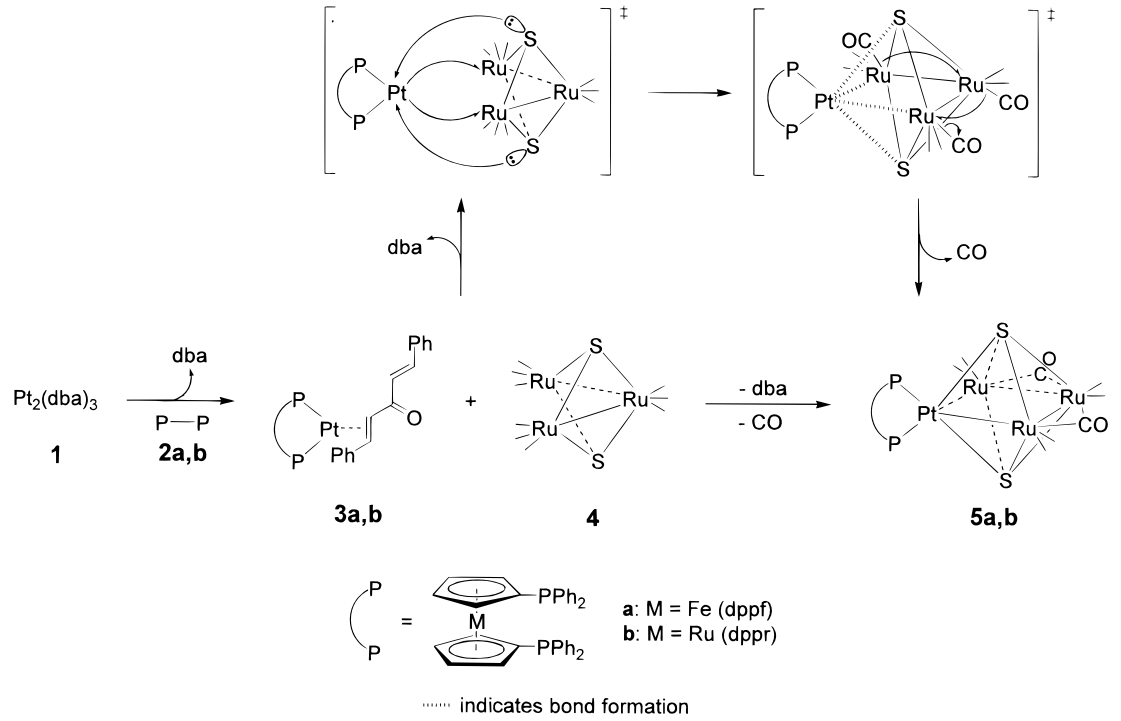

as sources of [Pt(P−P)] is illustrated by the facile reactions with $Ru_3(CO)_9(\mu_3\text{-}S)_2$ (**4**).[9] The structure of the resultant clusters, the unusual bonding modes of sulfide, the mechanistic implications, and some notable differences with earlier work are discussed in this paper.

Results and Discussion

$Pt_2(dba)_3$ (**1**) is easily accessible from K_2PtCl_4 and dba.[10] Substitution of **1** with 2 equiv of dppf (**2a**)[4] and dppr (**2b**)[5] at room temperature in toluene yields the orange complex Pt(η^2-P−P)(η^2-dba) [P−P = dppf (**3a**) or dppr (**3b**)] (Scheme 1). The $^{31}P\{^1H\}$ NMR spectrum at room temperature reveals an AX pattern for two inequivalent phosphines. This is consistent with an asymmetric disposition of the dba ligand through the coordination of one of two available C=C groups, instead of through a symmetric contact at the α,α′-unsaturated CO site. This is supported by IR analyses that give ν(CO) bands (**3a**, 1646; **3b**, 1646 cm^{-1}) similar to those of free dba (1651 cm^{-1}). As there is only one dba complex in this series, viz. Pd(η^2-dppe)(η^2-dba) that has been crystallographically characterized,[11] with no precedent in the literature on any Pt analogues, we have undertaken a single-crystal X-ray diffraction analysis of **3a** (Figure 1). It confirmed a mononuclear structure with chelating dppf and dba coordinated through one C=C group, giving a planar geometry (dihedral angle between the P(1)−Pt−P(2) and C(17)−Pt−C(18) planes is 6.5°). The coordinated C−C bond (1.431(4) Å) is necessarily longer than the dangling one (1.317(5) Å). When compared to other analogous Pt(PR_3)$_2$(η^2-alkene) complexes (Table 1),[12] the C(17)−C(18) bond length is relatively short, while the Pt−C lengths are long. The structural data advocate a more olefinic C=C group binding to a formally Pt(0) center, and facile dissociation of dba enables **3a** to function as a valuable source of [Pt(dppf)]. The striking similarity of the C−C and Pt−C lengths and other key structural parameters of **3a** and Pt-

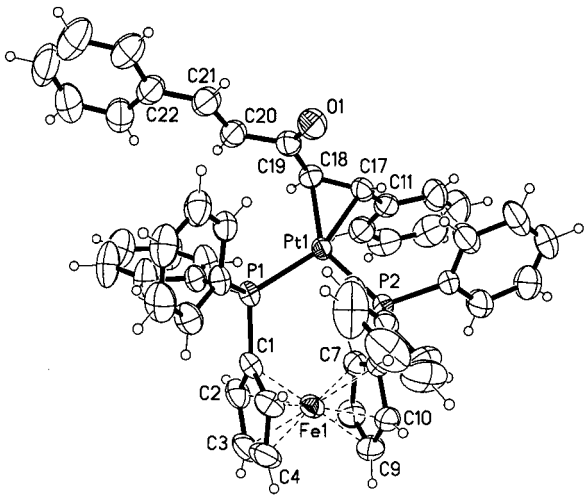

Figure 1. Crystal structure of Pt(η^2-dppf)(η^2-dba) (**3a**), with thermal ellipsoids at 50% probability.

(9) (a) Adams, R. D.; Babin, J. E. *Inorg. Chem.* **1986**, *25*, 4010. (b) Adams, R. D.; Babin, J. E.; Tasi, M. *Inorg. Chem.* **1986**, *25*, 4514.

(10) (a) Lewis, L. N.; Krafft, T. A.; Huffman, J. C. *Inorg. Chem.* **1992**, *31*, 3555. (b) Moseley, K.; Maitlis, P. M. *J. Chem. Soc., Chem. Commun.* **1971**, 982. (c) Takahashi, Y.; Ito, T.; Ishii, Y. *J. Chem. Soc., Chem. Commun.* **1970**, 1065.

(11) Herrmann, W. A.; Thiel, W. R.; Brossmer, C.; Öfele, K.; Priermeier, T.; Scherer, S. *J. Organomet. Chem.* **1993**, *461*, 51.

(12) (a) Baker, M. J.; Harrison, K. N.; Orpen, A. G.; Pringle, P. G.; Shaw, G. *J. Chem. Soc., Dalton Trans.* **1992**, 2607. (b) Clark, H. C.; Ferguson, G.; Hampden-Smith, M. J.; Kaitner, B.; Rügger, H. *Polyhedron* **1988**, *7*, 1349. (c) Bombieri, G.; Forsellini, E.; Panattoni, C.; Graziani, R.; Bandolis, G. *J. Chem. Soc. A* **1970**, 1313. (d) Francis, J. N.; McAdam, A.; Ibers, J. A. *J. Organomet. Chem.* **1971**, *29*, 131. (e) McAdam, A.; Francis, J. N.; Ibers, J. A. *J. Organomet. Chem.* **1971**, *29*, 149. (f) Christofides, A.; Howard, J. A. K.; Spencer, J. L.; Stone, F. G. A. *J. Organomet. Chem.* **1982**, *232*, 279. (g) Choi, H.; Hershberger, J. W.; Pinhas, A. R.; Ho, D. M. *Organometallics* **1991**, *10*, 2930. (h) Rheingold, A. L.; Baldacchini, C. J.; Macklin, P. D.; Geoffroy, G. L. *Acta Crystallogr., Sect. C* **1990**, *46*, 496.

Table 1. Comparison of Selected Bond Distances (Å) and Angles (deg) of the $PtC^1C^2P^1P^2$ Skeleton in $Pt(\eta^2\text{-dppf})(\eta^2\text{-dba})$ (3a) and Some Complexes of Type $Pt(PR_3)_2(\eta^2\text{-alkene})$

	bond lengths			bond angles		dihedral angle	
complex	C^1-C^{2a}	mean Pt−C	mean Pt−P	C^1-Pt-C^2	P^1-Pt-P^2	$P^1-Pt-P^2\cdots C^1-Pt-C^2$	ref
$Pt(\eta^2\text{-dppf})(\eta^2\text{-dba})$ (**3a**)	1.431(4)	2.134(3)	2.2665(8)	39.18(12)	100.72(3)	6.5	this work
$Pt(PPh_3)_2(\eta^2\text{-}C_2H_4)$	1.434(13)	2.111(9)	2.268(2)	39.7(4)	111.6(1)	1.6	2b
$Pt[P(O\text{-}2\text{-}C_6H_4OMe)_3]_2(\eta^2\text{-}C_2H_4)$	1.417(7)	2.130(5)	2.228(2)	38.9(2)	105.8(1)	2.5	12a
$Pt(PCy_3)_2(\eta^2-C_2H_4)$	1.440(7)	2.137(7)	2.284(1)	39.4(2)	116.33(7)	2.6	12b
$Pt(PPh_3)_2[\eta^2\text{-}C_2(CN)_4]$	1.49(5)	2.11(3)	2.290(9)	41.5(13)	101.4(3)	8.3	12c
$Pt(PPh_3)_2(\eta^2\text{-}C_2Cl_4)$	1.62(3)	2.04(3)	2.285(8)	47.1(1)	100.6(2)	12.3	12d
$Pt(PPh_3)_2(\eta^2\text{-}Cl_2C{=}C(CN)_2)$	1.42(3)	2.05(2)	2.300(6)	40.6(9)	102.0(2)	1.9	12e
$Pt(PPh_3)_2(\eta^2\text{-}C_{18}H_{14})$	1.52(3)	2.20(2)	2.291(6)	40.5(7)	103.8(2)	5.0	12f
$Pt(PPh_3)_2(\eta^2\text{-}C_{10}H_{12}O_4)$	1.486(9)	2.109(6)	2.292(2)	41.2(2)	105.5(1)	6.4	12g
$Pt(PPh_3)_2(\eta^2\text{-}C_{12}H_{19}O_2N)$	1.451(13)	2.146(8)	2.313(2)	39.5(3)	106.6(1)	11.4	12h

[a] C^1-C^2 denotes C−C bond distance (Å) of coordinated C=C group.

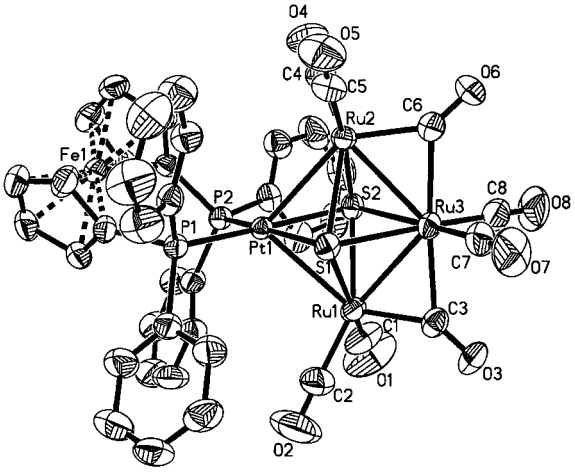

Figure 2. Crystal structure of $PtRu_3(CO)_6(\mu\text{-}CO)_2(\eta^2\text{-dppf})(\mu_4\text{-}S)_2$ (**5a**), with thermal ellipsoids at 50% probability.

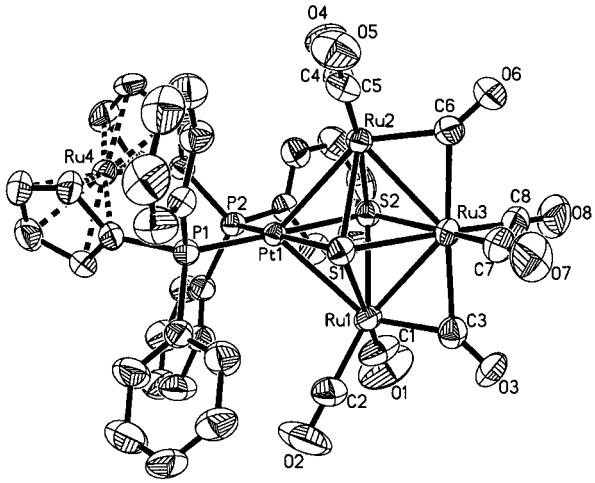

Figure 3. Crystal structure of $PtRu_3(CO)_6(\mu\text{-}CO)_2(\eta^2\text{-dppr})(\mu_4\text{-}S)_2$ (**5b**), with thermal ellipsoids at 50% probability.

$(PPh_3)_2(\eta^2\text{-}C_2H_4)$ (Table 1) further indicate that it is probably as labile as the latter and its chemistry as rich.

Stoichiometric addition of **3** to **4** in dry toluene at −40 °C gives $PtRu_3(CO)_6(\mu\text{-}CO)_2(\eta^2\text{-P−P})(\mu_4\text{-}S)_2$ [P−P = dppf (**5a**) or dppr (**5b**)] (Scheme 1) in very reasonable yields (82% and 57%, respectively). $^{31}P\{^1H\}$ NMR and IR analyses suggest that both structures are probably isostructural, with the diphosphine staying on the Pt center ($^1J_{P-Pt}$ = 3493 Hz in **5a** and 3564 Hz in **5b**) and that both terminal and bridging carbonyls are present. The crystal structures of clusters **5a** (Figure 2) and **5b** (Figure 3) are indeed isomorphous and isostructural, showing an approximately square heterometallic $\{PtRu_3\}$ core supported by two strong Ru−Ru (**5a**, av 2.7478(5) Å; **5b**, av 2.7463(7) Å), two strong Pt−Ru bonds (**5a**, av 2.8627(4) Å; **5b**, av 2.8620(6) Å), and two symmetrically capping μ_4-sulfide ligands above and below the $PtRu_3$ plane. In both compounds, there are two terminal carbonyls on each Ru, a carbonyl group edge-bridging each Ru−Ru bond, and a chelating dppf (**5a**) or dppr (**5b**) on the Pt center. The solid-state structures are thus in agreement with the solution spectroscopic data. Each $\{PtRu_3S_2\}$ cluster core can be described as a "compressed octahedron" with the S(1)···S(2) distance (**5a**, 3.033 Å; **5b**, 3.029 Å) being significantly shorter than the M−M distances [Pt(1)···Ru(3), 3.905 Å (**5a**) and 3.901 Å (**5b**); Ru(1)···Ru(2), 4.025 Å (**5a**) and 4.026 Å (**5b**)]. These 62e$^-$ square clusters can be treated as the *arachno* derivatives (cf. a 62e$^-$ square, $Ru_4(CO)_{11}(\mu_4\text{−}PPh)_2$)[13] of a *closo* 86e$^-$ octahedral cluster (e.g., $Rh_6(CO)_{16}$) and hence in compliance with the predictions of PSEPT.[14] The presence of only four M−M bonds is however one short of the alternative *arachno* butterfly form or one that is in adherence to 18e$^-$ rule. When **5a** and **5b** are compared with a related cluster, $PtRu_3(CO)_9(PPh_3)_2(\mu_3\text{-}S)_2$ (**7**)[15] (av Ru−Ru 2.8979(5) Å and av Pt−Ru 2.9081(4) Å),[3b] which has two additional electrons but the same number of M−M bonds, it is apparent that all the M−M bonds in **5a** and **5b** are shorter by 5.2% and 1.6% in the Ru−Ru and Pt−Ru bonds, respectively. This increase in bonding interaction provides an alternative for clusters **5a** and **5b** to achieve stabilization without formally giving a butterfly structure or adhering to the 18e$^-$ rule. The shorter Ru−Ru bonds also facilitate the formation of bridging CO ligands between Ru(1)−Ru(3) and Ru(2)−Ru(3). Furthermore, since **5a** and **5b** are isostructural, they provide an ideal comparison of the bonding parameters of dppf and dppr in chelating mode. The bite angle of dppr (99.63(6)°) is 2.1% larger than that of dppf (97.55(5)°), while the average $M\cdots Cp_{centroid}$ (M = Fe, Ru) distance in dppr (1.805 Å) is 9.6% larger than in dppf (1.647 Å). The bite angle of a phosphine has been linked to the catalytic efficiency of its complexes.[5b,16]

(13) (a) Field, J. S.; Haines, R. J.; Smit, D. N. *J. Organomet. Chem.* **1982**, *224*, C49. (b) Field, J. S.; Haines, R. J.; Smit, D. N. *J. Chem. Soc., Dalton Trans.* **1988**, 1315.

(14) Mingos, D. M. P. *Acc. Chem. Res.* **1984**, *17*, 311.

(15) This cluster was reported by Adams in a similar reaction[3b] and also obtained by us from **4** and $Pt(PPh_3)_2(dba)$.

Another interesting feature of **5a** and **5b** is the presence of two μ_4-sulfido ligands symmetrically capping above and below the heterometallic metal plane. Such clusters with the sulfides adopting an "inverted umbrella" configuration,[17] essentially denoting a $4e^-$ donor sulfide (as opposed to a tetrahedral $6e^-$ donor), are uncommon. Examples include $Fe_2Co_2(CO)_{10}(\mu\text{-}CO)(\mu_4\text{-}S)_2$,[18] $[Fe_2Mo_2(CO)_{10}(\mu\text{-}CO)_2(\mu_4\text{-}S)_2]^{2-}$,[19] and $WRu_3(CO)_9(\mu\text{-}CO)_2(PPhMe_2)(\mu_4\text{-}S)_2$.[20] More common are those with only one μ_4-S ligand, e.g., $[HPtOs_3(CO)_8(\mu_4\text{-}S)(\mu_3\text{-}S)(PPh_2C_6H_4)]_2$,[21] $[Fe_3Mn(CO)_{12}(\mu_4\text{-}S)]^-$,[22] and $Ru_5(CO)_{15}(\mu_4\text{-}S)$.[23]

From a mechanistic viewpoint, it is reasonable to suggest that **5** is a primary product resulting from a "two-pronged" capture of the unsaturated [Pt(P−P)] fragment by the two sulfide lone pairs as the latter approaches the most sterically favored "open" end of the $\{Ru_3S_2\}$ tbp, where there is no Ru−Ru bond (Scheme 1). This results in the direct formation of two Pt−S and two Pt−Ru bonds without disturbing the rest of the cluster core, apart from some electron density shift leading to CO migrations and elimination. This mode of attack accounts for the formation of the observed $\{M_4S_2\}$ octahedron and provides an alternative to the earlier proposal whereby the initial attack occurs at the tip of the tbp involving only one sulfide ligand. The significant shift of the M−S (M = Ru and Os) electron density to form the Pt−S bonds, cleavage of the M−M bonds, and associated cluster reorganization are also not observed here. In the course of reaction, the diphosphine ligand remains on the Pt center without hopping over to the neighboring Ru centers. This is not surprising since these metallocenyl ligands are known to be most stable in the chelating form and least so when bridging a short M−M bond.[4a,b] The resultant formation of a metal plane connected by M−M bonds discourages such migration, thereby stopping the phosphine substitution reactions that are common in the related Ru and Os reactions when PPh_3 is used. With the use of such a diphosphine in **3**, it is unlikely that free phosphine could be released in any significant quantity, and hence the subsequent re-entry of the phosphine is largely prohibited. Such secondary attack from adventitious phosphine could lead to changes in the electronic and steric environment and promote further cluster transformation. The present lack of isolable byproducts could be a result of these favorable conditions. However, if the reaction is carried out in "one pot" containing a mixture of **1**, **2**, and **4** (1:2:2), the yield of **5** is poor, while $Ru_3(CO)_7(\mu\text{-}P\text{−}P)(\mu_3\text{-}S)_2$ [P−P = dppf (**6a**) or dppr (**6b**)] would form as a significant byproduct. The crystal

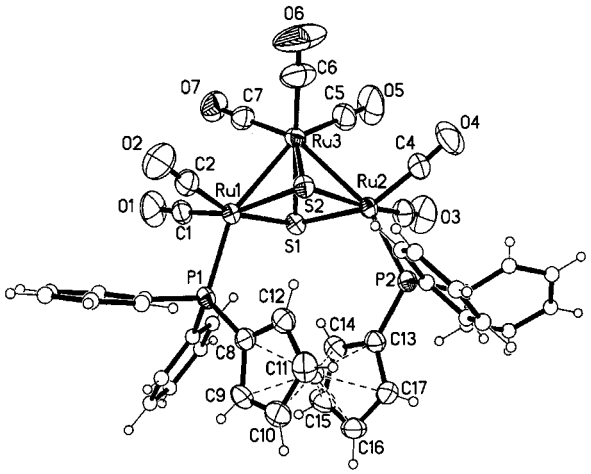

Figure 4. Crystal structure of $Ru_3(CO)_7(\mu\text{-dppf})(\mu_3\text{-}S)_2$ (**6a**), with thermal ellipsoids at 50% probability.

structure of **6a** reveals that the dppf ligand is bridging across the open end of the Ru_3 triangle (Figure 4). This further demonstrates that dppf prefers not to traverse across a Ru−Ru bond. It also supports our suggestion that formation of **5** is a result of the approach of the Pt fragment toward the Ru···Ru nonbonding site on the equatorial plane of the $\{Ru_3S_2\}$ pyramid. When this entry is blocked by a diphosphine ligand (as in **6**), the likelihood of such attack is significantly diminished, and this accounts for the poor yield of **5** in the one pot reactions. To verify this, a 1:1 mixture of **6** and **3** gives negligible yield of **5**, thus proving that dppf is not labile in these complexes and that formation of **5** demands an easy access somewhere along the midpoint of the two sulfide ligands.

Experimental Section

General Procedures. All reactions were performed under pure dry argon using standard Schlenk techniques. $Pt_2(dba)_3$ (**1**),[10] dppf (**2a**),[4] dppr (**2b**),[5b] and $Ru_3(CO)_9(\mu_3\text{-}S)_2$ (**4**)[9] were prepared by literature methods. Solvents used were of reagent grade and were dried by published procedures[24] and freshly distilled and degassed under argon before use. All other reagents were commercial products and were used as received. Precoated silica TLC plates of layer thickness 0.25 mm were obtained from Merck or Baker. All IR spectra were recorded on a Perkin-Elmer 1600 FT-IR spectrometer. ^1H and $^{31}P\{^1H\}$ NMR spectra were recorded on a Bruker ACF 300 MHz spectrometer at ca. 300 K at field strengths of 300.0 and 121.5 MHz, respectively. ^1H and ^{31}P chemical shifts are quoted in ppm downfield of tetramethylsilane and externally referenced to 85% H_3PO_4, respectively. Elemental analyses were performed by the Microanalytical Laboratory, Department of Chemistry, National University of Singapore. The presence of solvate molecules in **5a** and **5b** was confirmed by NMR analysis. The solvent inclusion in the crystal lattice of many dppf complexes has been noted in the literature.[25]

Synthesis. Pt(η^2-dppf)(η^2-dba) (3a). Solid **2a** (0.2160 g, 0.3804 mmol) was added to a solution of freshly prepared **1** (0.1040 g, 0.0951 mmol) in toluene (20 mL). The resulting wine-red solution was stirred at room temperature under argon for ca. 14 h, during which the solution turned clear

(16) (a) Hamann, B. C.; Hartwig, J. F. *J. Am. Chem. Soc.* **1998**, *120*, 3694. (b) Mann, G.; Baranano, D.; Hartwig, J. F.; Rheingold, A. L.; Guzei, I. A. *J. Am. Chem. Soc.* **1998**, *120*, 9205.

(17) Detailed descriptions of various bonding modes of sulfido ligands are given in: (a) Vahrenkamp, H. *Angew. Chem., Int. Ed. Engl.* **1975**, *14*, 322. (b) Vahrenkamp, H. *Angew. Chem., Int. Ed. Engl.* **1978**, *17*, 444.

(18) Vahrenkamp, H.; Wucherer, E. J. *Angew. Chem., Int. Ed. Engl.* **1981**, *20*, 680.

(19) Eldredge, P. A.; Bose, K. A.; Barber, D. E.; Bryan, R. F.; Sinn, E.; Rheingold, A. L.; Averill, B. A. *Inorg. Chem.* **1991**, *30*, 2365.

(20) Adams, R. D.; Wolfe, T. A.; Wu, W. *Polyhedron* **1991**, *10*, 447.

(21) Adams, R. D.; Hor, T. S. A. *Organometallics* **1984**, *3*, 1915.

(22) Schauer, C. K.; Harris, S.; Sabat, M.; Voss, E. J.; Shriver, D. F. *Inorg. Chem.* **1995**, *34*, 5017.

(23) Adams, R. D.; Babin, J. E.; Tasi, M. *Organometallics* **1988**, *7*, 503.

(24) Gordon, A. J.; Ford, R. A. *The Chemist's Companion: A Handbook of Practical Data, Techniques and References*; Wiley-Interscience: New York, 1972.

(25) Butler, I. R.; Cullen, W. R.; Kim, T. J.; Rettig, S. J.; Trotter, J. *Organometallics* **1985**, *4*, 972.

orange. The solvent was removed under reduced pressure, and the solid residue obtained was redissolved in a minimum amount of CH_2Cl_2 and chromatographed on silica TLC plates. Elution with CH_2Cl_2/acetone/hexane (1:1:8) gave two major bands: the yellow band (R_f 0.36) belongs to excess dba; a major orange band (R_f 0.07) was extracted with acetonitrile and recrystallized at 0 °C to yield orange crystals of complex **3a** (0.1208 g, 65%). Anal. Calcd for $C_{51}H_{42}FeOP_2Pt$: C, 62.3; H, 4.3; P, 6.3. Found: C, 62.0; H, 4.2; P, 6.2. IR (KBr disk) (cm^{-1}): 1652 (s), 1646 (s), 1637 (s, sh), 1594 (vs), 1560 (m), 1434 (s). $^{31}P\{^1H\}$ NMR ($CDCl_3$): $\delta_{P(1)}$ 21.1 (d), $\delta_{P(2)}$ 23.7 (d) [$^1J_{Pt-P(1)} = 3603$, $^1J_{Pt-P(2)} = 4273$, $^2J_{P(1)-P(2)} = 16$ Hz]. ^1H NMR ($CDCl_3$): δ_H 4.00−4.25 (m, 8 H, 2 C_5H_4), 3.75−4.20 (m, 2 H, coordinated olefin), 6.16 (d, 1 H, uncoordinated olefin α-H), and 7.05−7.68 (m, 31 H, 6 C_6H_5 and uncoordinated olefin β-H).

Pt(η^2-dppr)(η^2-dba) (3b). An analogous reaction as above using solid **2b** (75.7 mg, 0.1260 mmol) and **1** (46.0 mg, 0.0421 mmol) in toluene (20 mL) gave a clear yellow solution after stirring for 14 h under argon. TLC separation with CH_2Cl_2/acetone/hexane (1:1:8) also gave two major bands: the yellow band (R_f 0.36) belongs to excess dba; a major yellow band (R_f 0.08) was extracted with acetonitrile and recrystallized at 0 °C to yield complex **3b** (46.5 mg, 54%). Anal. Calcd for $C_{51}H_{42}OP_2PtRu$: C, 59.5; H, 4.1; P, 6.0. Found: C, 59.3; H, 4.0; P, 5.9. IR (KBr disk) (cm^{-1}): 1652 (s), 1646 (s), 1637 (s, sh), 1595 (vs), 1559 (m), 1434 (s). $^{31}P\{^1H\}$ NMR ($CDCl_3$): $\delta_{P(1)}$ 21.8 (d), $\delta_{P(2)}$ 24.6 (d) [$^1J_{Pt-P(2)} = 4397$, $^1J_{Pt-P(1)} = 3709$, $^2J_{P(1)-P(2)} = 15$ Hz]. ^1H NMR ($CDCl_3$): δ_H 4.42−4.69 (m, 8 H, 2 C_5H_4), 3.85−4.01 (m, 2 H, coordinated olefin), 5.94 (d, 1 H, uncoordinated olefin α-H), and 6.59−7.62 (m, 31 H, 6 C_6H_5 and uncoordinated olefin β-H).

PtRu$_3$(CO)$_6$(μ-CO)$_2$(η^2-dppf)(μ_4-S)$_2$ (5a). When solid **3a** (46.0 mg, 0.0468 mmol) was introduced into a solution of **4** (28.9 mg, 0.0468 mmol) in toluene (20 mL) immersed in an acetonitrile/N_2 bath at ca. −40 °C, and the orange solution darkened to a deep orange-red after 5 min. The mixture was stirred at this temperature for 1 h and then at 0 °C for another hour. The solvent was then removed under reduced pressure, and the solid residue obtained was redissolved in a minimum amount of CH_2Cl_2 and chromatographed on silica TLC plates. Elution with CH_2Cl_2/acetone/hexane (1:1:8) gave one major reddish band (R_f 0.34), which was extracted with CH_2Cl_2, layered with pentane, and recrystallized at 0 °C to give cluster **5a** (51.4 mg, 82%). Anal. Calcd for $C_{42}H_{28}FeO_8P_2PtRu_3S_2 \cdot CH_2Cl_2 \cdot 0.5C_5H_{12}$: C, 37.6; H, 2.1; P, 4.6. Found: C, 37.7; H, 2.5; P, 4.2. IR ($CHCl_3$) (cm^{-1}): ν(CO) 2055 (s), 2000 (vs), 1943 (s); ν(μ-CO) 1829 (m). $^{31}P\{^1H\}$ NMR ($CDCl_3$): δ_P 21.3 [s, $^1J_{P-Pt} = 3493$ Hz]. ^1H NMR ($CDCl_3$): δ_H 4.56 (m, 4 H, C_5H_4), 4.78 (m, 4 H, C_5H_4), and 7.30−7.93 (m, 20 H, C_6H_5).

PtRu$_3$(CO)$_6$(μ-CO)$_2$(η^2-dppr)(μ_4-S)$_2$ (5b). An analogous reaction using solid **3b** (21.5 mg, 0.0209 mmol) was introduced into a solution of **4** (12.9 mg, 0.0209 mmol) in toluene (20 mL) immersed in an acetonitrile/N_2 bath at ca. −40 °C, and the orange solution darkened to a deep orange-brown after 5 min. Similarly, the reaction mixture was stirred at this temperature for 1 h and then at 0 °C for another 1 h. TLC separation with CH_2Cl_2/acetone/hexane (1:1:8) gave one major red band (R_f 0.19), which was extracted with CH_2Cl_2, layered with pentane, and crystallized at 0 °C to give cluster **5b** (16.5 mg, 57%). Anal. Calcd for $C_{42}H_{28}O_8P_2PtRu_4S_2$: C, 36.4; H, 2.0; P, 4.5. Found: C, 36.4; H, 2.1; P, 4.2. IR ($CHCl_3$) (cm^{-1}): ν(CO) 2055 (s), 2000 (vs), 1944 (s); ν(μ-CO) 1829 (m). $^{31}P\{^1H\}$ NMR ($CDCl_3$): δ_P 20.6 [s, $^1J_{P-Pt} = 3564$ Hz]. ^1H NMR ($CDCl_3$): δ_H 5.10 (m, 4 H, C_5H_4), 5.30 (m, 4 H, C_5H_4), and 7.13−7.95 (m, 20 H, C_6H_5).

Ru$_3$(CO)$_7$(μ-dppf)(μ_3-S)$_2$ (6a). Solid **4** (20.0 mg, 0.0323 mmol) was introduced into a solution of **2a** (17.9 mg, 0.0323 mmol) in toluene (20 mL), and the mixture was stirred at room temperature for 2 h. The solvent was removed under reduced pressure, and the solid residue obtained was redissolved in a minimum amount of CH_2Cl_2 and chromatographed on silica TLC plates. Elution with CH_2Cl_2/acetone/hexane (1:1:8) gave one major orange band (R_f 0.40), which was extracted with CH_2Cl_2, layered with *n*-hexane, and crystallized at 0 °C to give orange-red crystals of **6a** (23.0 mg, 64%). Anal. Calcd for $C_{41}H_{28}FeO_7P_2Ru_3S_2$: C, 44.1; H, 2.5; P, 5.5. Found: C, 43.9; H, 2.5; P, 5.4. IR (KBr disk) (cm^{-1}): ν(CO) 2053 (vs), 2022 (s), 2003 (s, sh), 1989 (s), 1974 (s), 1955 (s), 1946 (s, sh). $^{31}P\{^1H\}$ NMR ($CDCl_3$): δ_P 53.0 (s). ^1H NMR ($CDCl_3$): δ_H 3.16−5.06 (m, 8 H, C_5H_4) and 7.12−8.04 (m, 20 H, C_6H_5).

Ru$_3$(CO)$_7$(μ-dppr)(μ_3-S)$_2$ (6b). An analogous reaction was carried out using solid **4** (20.0 mg, 0.0323 mmol) and a solution of **2b** (19.4 mg, 0.0323 mmol) in toluene (20 mL). TLC separation with CH_2Cl_2/acetone/hexane (1:1:8) gave one major orange band (R_f 0.34), which was extracted with CH_2Cl_2, layered with *n*-hexane, and recrystallized at 0 °C to give orange crystals of **6b** (21.0 mg, 56%). Anal. Calcd for $C_{41}H_{28}O_7P_2Ru_4S_2$: C, 42.3; H, 2.4; P, 5.3. Found: C, 41.9; H, 2.4; P, 5.2. IR (KBR disk) (cm^{-1}): ν(CO) 2080 (s), 2046 (vs), 2028 (s, sh), 2008 (s), 1992 (s, sh), 1976 (s), 1966 (s, sh). $^{31}P\{^1H\}$ NMR ($CDCl_3$): δ_P 50.0 (s). ^1H NMR ($CDCl_3$): δ_H 4.38−4.70 (m, 8 H, C_5H_4) and 7.33−7.46 (m, 20 H, C_6H_5).

In Toto Reaction between Pt$_2$(dba)$_3$ (1), dppf (2a), and Ru$_3$(CO)$_9$(μ_3-S)$_2$ (4). Solid **4** (25.2 mg, 0.0407 mmol) was added to a wine-red solution of **1** (22.2 mg, 0.0204 mmol) and **2a** (22.6 mg, 0.0407 mmol) in toluene (20 mL). The solution, shielded from direct light, was stirred for ca. 2 h at room temperature. The resulting orange-brown solution was filtered, and the solvent was removed in vacuo. The residue was then redissolved in a minimum amount of CH_2Cl_2 and chromatographed on silica TLC plates. Elution with CH_2Cl_2/acetone/hexane (1:1:8) gave three major bands, which were extracted with CH_2Cl_2 and recrystallized from a CH_2Cl_2/hexane mixture to give, in order of decreasing R_f value, **6a** (R_f 0.40; 19.1 mg, 42%), **5a** (R_f 0.34; 9.1 mg, 15%), and **3a** (R_f 0.07; 4.4 mg, 11%).

In Toto Reaction between Pt$_2$(dba)$_3$ (1), dppr (2b), and Ru$_3$(CO)$_9$(μ_3-S)$_2$ (4). A similar reaction was carried out with solid **4** (29.6 mg, 0.0478 mmol) and a wine-colored solution of **1** (26.1 mg, 0.0239 mmol) and **2b** (28.7 mg, 0.0478 mmol) in toluene (20 mL). TLC separation with CH_2Cl_2/acetone/hexane (1:1:8) gave three major bands, which were extracted with CH_2Cl_2 and recrystallized from a CH_2Cl_2/hexane mixture to give, in order of decreasing R_f value, **6b** (R_f 0.34; 18.0 mg, 33%), **5b** (R_f 0.19; 7.9 mg, 11%), and **3b** (R_f 0.07; 4.1 mg, 8%).

X-ray Crystallography. The crystallographic data and structure refinement details for **3a**, **5a**, **5b**, and **6a** are given in Table 2; selected bond lengths and angles are given in Tables 3−6. The intensities were measured on a Bruker AXS SMART diffractometer, equipped with a CCD detector, using Mo Kα radiation ($\lambda = 0.71073$ Å) at 293(2) K. The software SMART[26] was used for collecting frames of data, indexing reflections, and determination of lattice parameters, SAINT[26] for integration of intensity of reflections and scaling, SADABS[27] for empirical absorption correction, and SHELXTL[28] for space group and structure determination, refinements, graphics, and structure reporting.

Pt(η^2-dppf)(η^2-dba) (3a). Orange crystals of complex **3a** were grown from a sample solution in acetonitrile by slow evaporation at room temperature (25 °C). A suitable single crystal of dimensions 0.5 × 0.48 × 0.36 mm^3 was mounted at the end of a glass fiber. A total of 18 581 reflections were collected in the θ range 2.27−29.29° ($-13 \le h \le 12$, $-13 \le k \le 13$, $-31 \le l \le 32$). For $Z = 2$, the space group $P\bar{1}$ was chosen in the triclinic system. All non-hydrogen atoms in the neutral molecule were refined anisotropically. A riding model was used to place the hydrogen atoms in their idealized positions. In

(26) *SMART & SAINT Software Reference Manuals*, version 4.0; Siemens Energy & Automation, Inc., Analytical Instrumentation: Madison, WI, 1996.

(27) Sheldrick, G. M. *SADABS, A Software for Empirical Absorption Correction*; University of Göttingen, 1996.

(28) *SHELXTL V*ersion 5.03; Siemens Energy and Automation Inc., Analytical Instrumentation: Madison, WI, 1996.

Table 2. Crystallographic Data for Pt(η^2-dppf)(η^2-dba) (3a), $PtRu_3(CO)_6(\mu\text{-}CO)_2(\eta^2\text{-dppf})(\mu_4\text{-}S)_2$ (5a)·CH_2Cl_2·0.5C_5H_{12}, $PtRu_3(CO)_6(\mu\text{-}CO)_2(\eta^2\text{-dppr})(\mu_4\text{-}S)_2$ (5b)·0.5CH_2Cl_2·0.5C_5H_{12}, and $Ru_3(CO)_7(\mu\text{-dppf})(\mu_3\text{-}S)_2$ (6a)

	3a	5a·CH_2Cl_2·0.5C_5H_{12}	5b·0.5CH_2Cl_2·0.5C_5H_{12}	6a
formula	$C_{51}H_{42}FeOP_2Pt$	$C_{46}H_{36}Cl_2FeO_8P_2PtRu_3S_2$	$C_{45}H_{40}ClO_8P_2PtRu_4S_2$	$C_{41}H_{28}FeO_7P_2Ru_3S_2$
fw	983.73	1467.86	1469.65	1117.75
cryst syst	triclinic	triclinic	triclinic	monoclinic
a (Å)	9.667(1)	13.9108(3)	13.8788(1)	11.3338(2)
b (Å)	9.877(1)	13.9292(3)	13.8701(2)	17.0153(2)
c (Å)	24.028(4)	14.7856(3)	14.7993(2)	22.7358(4)
α (deg)	85.41(1)	63.744(1)	64.393(1)	90
β (deg)	83.18(2)	75.201(1)	75.418(1)	104.32(1)
γ (deg)	65.21(1)	76.004(1)	76.051(1)	90
V (Å^3)	2066.9(5)	2456.55(9)	2457.59(5)	4248.3(1)
Z	2	2	2	4
ρ_{calcd} (g cm^{-3})	1.581	1.984	1.986	1.748
μ (mm^{-1})	3.847	4.336	4.291	1.602
no. of rflns collected	18 581	12 562	17 684	26 278
no. of indep rflns	9960	8295	8517	10 241
no. of rflns ≥ 2$\sigma(F_o)$	9455 (R_{int} = 0.0191)	7940 (R_{int} = 0.0183)	7431 (R_{int} = 0.0248)	8046 (R_{int} = 0.0462)
no. of params	505	573	580	506
Goof on $\|F\|^2$	1.160	1.089	1.179	1.026
R_1 and wR_2 (obs data)[a,b]	0.0261 and 0.0645	0.0312 and 0.0807	0.0340 and 0.0865	0.0471 and 0.1148
R_1 and wR_2 (all data)	0.0287 and 0.0660	0.0335 and 0.0838	0.0425 and 0.0906	0.0633 and 0.1237

[a] $R_1 = \sum||F_o| - |F_c||/\sum|F_o|$. [b] $wR_2 = \sqrt{\{\sum[w(F_o^2 - F_c^2)^2]/\sum[w(F_o^2)^2]\}}$, $w^{-1} = \sigma^2(F_o^2) + (aP)^2 + bP$.

Table 3. Selected Bond Lengths (Å) and Angles (deg) for 3a

Bond Distances

Pt(1)−C(17)	2.125(3)	C(11)−C(17)	1.474(5)
Pt(1)−C(18)	2.143(3)	C(18)−C(19)	1.449(5)
Pt(1)−P(1)	2.2762(8)	C(19)−C(20)	1.488(5)
Pt(1)−P(2)	2.2567(8)	C(21)−C(22)	1.464(5)
C(17)−C(18)	1.431(4)	mean Fe(1)−C(1−5)	2.040(4)
C(20)−C(21)	1.317(5)	mean Fe(1)−C(6−10)	2.042(4)
O(1)−C(19)	1.232(4)	mean Fe(1)···$Cp_{centroid}$	1.645

Bond Angles

C(17)−Pt(1)−C(18)	39.18(12)	C(18)−C(17)−Pt(1)	71.08(17)
P(1)−Pt(1)−P(2)	100.72(3)	C(11)−C(17)−Pt(1)	115.7(2)
C(17)−Pt(1)−P(1)	154.97(9)	C(19)−C(18)−Pt(1)	102.0(2)
C(17)−Pt(1)−P(2)	103.84(9)	C(17)−C(18)−C(19)	121.3(3)
C(18)−Pt(1)−P(1)	116.34(9)	C(18)−C(19)−C(20)	115.0(3)
C(18)−Pt(1)−P(2)	142.93(9)	O(1)−C(19)−C(18)	124.5(3)
C(17)−C(18)−Pt(1)	69.74(17)	O(1)−C(19)−C(20)	120.5(3)

Dihedral Angles

P(1)−Pt(1)−P(2)···C(17)−Pt(1)−C(18)	6.5
$Cp_{centroid}$(1)···Fe(1)···$Cp_{centroid}$(2)	177.6

the final least-squares refinement cycles on F^2, the model converged to $R_1 = 0.0261$, $wR_2 = 0.0645$, and $S = 1.160$ for 9960 observed reflections with $I > 2\sigma(I)$ and 505 parameters, and $R_1 = 0.0287$, $wR_2 = 0.0660$ for all 9960 data. In the final Fourier-difference map, the deepest hole was −0.591 e/Å^3 and the highest peak was 0.909 e/Å^3.

$PtRu_3(CO)_6(\mu\text{-}CO)_2(\eta^2\text{-dppf})(\mu_4\text{-}S)_2$ (5a). Deep-red crystals of complex **5a** were grown by layering a solution of the compound in dichloromethane with *n*-pentane in a freezer at −5 °C. A suitable single crystal of dimensions 0.24 × 0.22 × 0.08 mm^3 was selected, wedged inside a glass capillary tube, and flame-sealed. A total of 12 562 reflections were collected in the θ range 2.36−25.00° (−16 ≤ *h* ≤ 16, −16 ≤ *k* ≤ 12, −17 ≤ *l* ≤ 15). For *Z* = 2, the space group $P\bar{1}$ was chosen in the triclinic system. All non-hydrogen atoms in the neutral molecule were refined anisotropically. One disordered molecule of dichloromethane was located in the Fourier-difference synthesis (occupancy 0.5/0.5). Another severely distorted half-molecule of pentane was found in the asymmetric unit near the center of inversion. Both disorder models were successfully incorporated into the least-squares cycles. Ideal bond distances and angles were imposed for these dichloromethane and *n*-pentane solvates, and common isotropic thermal parameters were refined for each model. A riding model was used to place the hydrogen atoms in their idealized positions. In the final least-squares refinement cycles on F^2, the model converged to $R_1 = 0.0312$, $wR_2 = 0.0807$, and $S = 1.089$ for 8295 observed reflections with $I > 2\sigma(I)$ and 573 parameters, and $R_1 = 0.0335$, $wR_2 = 0.0838$ for all 8295 data. In the last Fourier-difference map, the deepest hole was −1.171 e/Å^3 and the highest peak was 0.992 e/Å^3.

Table 4. Selected Bond Lengths (Å) and Angles (deg) for 5a

Bond Distances

Ru(1)−Ru(3)	2.7451(6)	Pt(1)−P(1)	2.3094(13)
Ru(2)−Ru(3)	2.7506(6)	Pt(1)−P(2)	2.2779(12)
Ru(1)···Ru(2)	4.025	mean Ru(1)−C(1−2)	1.869(8)
Ru(1)−Pt(1)	2.8305(4)	mean Ru(2)−C(4−5)	1.867(6)
Ru(2)−Pt(1)	2.8949(4)	mean Ru(3)−C(7−8)	1.886(7)
Ru(3)···Pt(1)	3.905	Ru(1)−C(3)	1.966(6)
Ru(1)−S(1)	2.5295(14)	Ru(2)−C(6)	1.978(6)
Ru(1)−S(2)	2.5272(13)	Ru(3)−C(3)	2.215(6)
Ru(2)−S(1)	2.5860(13)	Ru(3)−C(6)	2.202(6)
Ru(2)−S(2)	2.4634(13)	mean C−O (terminal)	1.137(9)
Ru(3)−S(1)	2.5451(13)	mean C−O (bridging)	1.169(8)
Ru(3)−S(2)	2.5608(13)	mean Fe(1)−C(9−13)	2.046(7)
Pt(1)−S(1)	2.3900(12)	mean Fe(1)−C(14−18)	2.042(7)
Pt(1)−S(2)	2.3970(12)	mean Fe(1)···$Cp_{centroid}$	1.647
S(1)···S(2)	3.033		

Bond Angles

Ru(1)−Pt(1)−Ru(2)	89.319(13)	P(2)−Pt(1)−Ru(2)	120.68(3)
Pt(1)−Ru(1)−Ru(3)	88.910(15)	Pt(1)−S(1)−Ru(1)	70.18(4)
Pt(1)−Ru(2)−Ru(3)	87.498(15)	Pt(1)−S(1)−Ru(2)	71.03(3)
Ru(1)−Ru(3)−Ru(2)	94.164(17)	Pt(1)−S(1)−Ru(3)	104.58(5)
S(1)−Pt(1)−S(2)	78.62(4)	Ru(1)−S(1)−Ru(2)	103.76(5)
S(1)−Ru(1)−S(2)	73.70(4)	Ru(1)−S(1)−Ru(3)	65.49(3)
S(1)−Ru(2)−S(2)	73.78(4)	Ru(2)−S(1)−Ru(3)	64.82(3)
S(1)−Ru(3)−S(2)	72.88(4)	Pt(1)−S(2)−Ru(1)	70.12(4)
P(1)−Pt(1)−P(2)	97.55(5)	Pt(1)−S(2)−Ru(2)	73.10(4)
P(1)−Pt(1)−S(1)	92.93(5)	Pt(1)−S(2)−Ru(3)	103.89(5)
P(1)−Pt(1)−S(2)	170.75(5)	Ru(1)−S(2)−Ru(2)	107.49(5)
P(2)−Pt(1)−S(1)	168.28(5)	Ru(1)−S(2)−Ru(3)	65.30(3)
P(2)−Pt(1)−S(2)	91.22(5)	Ru(2)−S(2)−Ru(3)	66.35(3)
P(1)−Pt(1)−Ru(1)	121.24(3)	Ru(1)−C(3)−Ru(3)	81.9(2)
P(1)−Pt(1)−Ru(2)	117.66(4)	Ru(2)−C(6)−Ru(3)	82.1(2)
P(2)−Pt(1)−Ru(1)	112.26(3)		

Dihedral Angles

P(1)−Pt(1)−P(2)···S(1)−Pt(1)S(2)	6.7
P(1)−Pt(1)−P(2)···Ru(1)−Ru(2)−Ru(3)	94.9
S(1)−Pt(1)−S(2)···Ru(1)−Ru(2)−Ru(3)	88.5
Ru(1)−Pt(1)−Ru(2)···S(1)−Ru(3)−S(2)	88.6
$Cp_{centroid}$(1)···Fe(1)···$Cp_{centroid}$(2)	178.1

Table 5. Selected Bond Lengths (Å) and Angles (deg) for 5b

Bond Distances

Ru(1)−Ru(3)	2.7410(7)	Pt(1)−P(1)	2.3195(16)
Ru(2)−Ru(3)	2.7516(7)	Pt(1)−P(2)	2.2823(15)
Ru(1)···Ru(2)	4.026	mean Ru(1)−C(1−2)	1.865(9)
Ru(1)−Pt(1)	2.8294(6)	mean Ru(2)−C(4−5)	1.859(7)
Ru(2)−Pt(1)	2.8946(5)	mean Ru(3)−C(7−8)	1.878(8)
Ru(3)···Pt(1)	3.901	Ru(1)−C(3)	1.975(7)
Ru(1)−S(1)	2.5357(17)	Ru(2)−C(6)	1.966(7)
Ru(1)−S(2)	2.5289(16)	Ru(3)−C(3)	2.225(7)
Ru(2)−S(1)	2.5812(16)	Ru(3)−C(6)	2.186(7)
Ru(2)−S(2)	2.4587(16)	mean C−O (terminal)	1.140(9)
Ru(3)−S(1)	2.5462(17)	mean C−O (bridging)	1.167(8)
Ru(3)−S(2)	2.5571(16)	mean Ru(4)−C(9−13)	2.180(7)
Pt(1)−S(1)	2.3833(15)	mean Ru(4)−C(14−18)	2.170(7)
Pt(1)−S(2)	2.3943(16)	mean Ru(4)···$Cp_{centroid}$	1.805
S(1)···S(2)	3.029		

Bond Angles

Ru(1)−Pt(1)−Ru(2)	89.385(16)	P(2)−Pt(1)−Ru(2)	119.69(4)
Pt(1)−Ru(1)−Ru(3)	88.875(18)	Pt(1)−S(1)−Ru(1)	71.15(4)
Pt(1)−Ru(2)−Ru(3)	87.353(18)	Pt(1)−S(1)−Ru(2)	71.20(4)
Ru(1)−Ru(3)−Ru(2)	94.27(2)	Pt(1)−S(1)−Ru(3)	104.56(6)
S(1)−Pt(1)−S(2)	78.68(5)	Ru(1)−S(1)−Ru(2)	103.77(6)
S(1)−Ru(1)−S(2)	73.46(5)	Ru(1)−S(1)−Ru(3)	65.28(4)
S(1)−Ru(2)−S(2)	73.83(5)	Ru(2)−S(1)−Ru(3)	64.91(4)
S(1)−Ru(3)−S(2)	72.81(5)	Pt(1)−S(2)−Ru(1)	70.10(4)
P(1)−Pt(1)−P(2)	99.63(6)	Pt(1)−S(2)−Ru(2)	73.22(5)
P(1)−Pt(1)−S(1)	91.53(6)	Pt(1)−S(2)−Ru(3)	103.91(6)
P(1)−Pt(1)−S(2)	169.64(5)	Ru(1)−S(2)−Ru(2)	107.64(6)
P(2)−Pt(1)−S(1)	167.94(6)	Ru(1)−S(2)−Ru(3)	65.22(4)
P(2)−Pt(1)−S(2)	90.42(5)	Ru(2)−S(2)−Ru(3)	66.51(4)
P(1)−Pt(1)−Ru(1)	120.07(4)	Ru(1)−C(3)−Ru(3)	81.2(3)
P(1)−Pt(1)−Ru(2)	117.28(4)	Ru(2)−C(6)−Ru(3)	82.8(3)
P(2)−Pt(1)−Ru(1)	112.18(4)		

Dihedral Angles

P(1)−Pt(1)−P(2)···S(1)−Pt(1)−S(2)	5.8
P(1)−Pt(1)−P(2)···Ru(1)−Ru(2)−Ru(3)	94.2
S(1)−Pt(1)−S(2)···Ru(1)−Ru(2)−Ru(3)	88.6
Ru(1)−Pt(1)−Ru(2)···S(1)−Ru(3)−S(2)	88.6
$Cp_{centroid}$(1)···Ru(4)···$Cp_{centroid}$(2)	176.6

$PtRu_3(CO)_6(\mu$-CO$)_2(\eta^2$-dppr$)(\mu_4$-S$)_2$ (5b). Deep-orange crystals of complex **5b** were grown by layering a solution of the compound in dichloromethane with *n*-pentane in a freezer at −5 °C. A suitable single crystal of dimensions 0.5 × 0.38 × 0.30 mm^3 was selected, wedged inside a glass capillary tube, and flame-sealed. A total of 17 684 reflections were collected in the θ range 1.97−25.00° (−16 ≤ h ≤ 16, −14 ≤ k ≤ 16, −17 ≤ l ≤ 15). For $Z = 2$, the space group $P\bar{1}$ was chosen in the triclinic system. All non-hydrogen atoms in the neutral molecule were refined anisotropically. The lattice contains one dichloromethane and an *n*-pentane solvent molecule. Severe disorder is present in the solvent region; dichloromethane is present in two regions, and *n*-pentane is disordered (occupancy 0.5/0.5) near the center of inversion. A riding model was used to place the hydrogen atoms in their idealized positions. In the final least-squares refinement cycles on F^2, the model converged to $R_1 = 0.0340$, $wR_2 = 0.0865$, and $S = 1.179$ for 8517 observed reflections with $I > 2\sigma(I)$ and 580 parameters, and $R_1 = 0.0425$, $wR_2 = 0.0906$ for all 8517 data. In the last Fourier-difference map, the deepest hole was −0.532 e/Å^3 and the highest peak was 1.178 e/Å^3.

Table 6. Selected Bond Lengths (Å) and Angles (deg) for 6a

Bond Distances

Ru(1)−Ru(3)	2.7751(4)	mean Ru−S	2.4049(10)
Ru(2)−Ru(3)	2.7565(4)	mean Ru−C	1.894(6)
Ru(1)···Ru(2)	3.725	mean C−O (terminal)	1.138(7)
S(1)···S(2)	3.002	mean Fe(1)−C(8−12)	2.042(5)
Ru(1)−P(1)	2.3300(10)	mean Fe(1)−C(13−17)	2.047(5)
Ru(2)−P(2)	2.3203(10)	mean Fe(1)···$Cp_{centroid}$	1.650

Bond Angles

Ru(1)−Ru(3)−Ru(2)	84.650(12)	Ru(1)−S(2)−Ru(2)	103.11(4)
Ru(1)−S(1)−Ru(2)	100.92(4)	Ru(1)−S(2)−Ru(3)	70.66(3)
Ru(1)−S(1)−Ru(3)	70.00(3)	Ru(2)−S(2)−Ru(3)	70.03(3)
Ru(2)−S(1)−Ru(3)	69.48(3)		

Dihedral Angles

S(1)−Ru(3)−S(2)···Ru(1)−Ru(2)−Ru(3)	90.1
$Cp_{centroid}$(1)···Fe(1)···$Cp_{centroid}$(2)	176.7

$Ru_3(CO)_7(\mu$-dppf$)(\mu_3$-S$)_2$ (6a). Orange-red crystals of complex **6a** were grown by layering a solution of the compound in dichloromethane with *n*-hexane in a refrigerator at 5 °C. A suitable single crystal of dimensions 0.48 × 0.16 × 0.12 mm^3 was mounted at the end of a glass fiber. A total of 26 278 reflections were collected in the θ range 2.20−29.37° (−13 ≤ h ≤ 14, −21 ≤ k ≤ 23, −29 ≤ l ≤ 27). For $Z = 4$, the space group $P2_1/n$ was chosen in the monoclinic system. All non-hydrogen atoms in the neutral molecule were refined anisotropically. A riding model was used to place the hydrogen atoms in their idealized positions. In the final least-squares refinement cycles on F^2, the model converged to $R_1 = 0.0471$, $wR_2 = 0.1148$, and $S = 1.026$ for 10 241 observed reflections with $I > 2\sigma(I)$ and 506 parameters, and $R_1 = 0.0633$, $wR_2 = 0.1237$ for all 10 241 data. In the final Fourier-difference map, the deepest hole was −1.746 e/Å^3 and the highest peak was 1.443 e/Å^3.

Acknowledgment. The authors thank the National University of Singapore (NUS) (Grant No. RP 960664/A) for financial support and the technical staff in the Department of Chemistry of NUS for supporting services. S.-W.A.F. is grateful to NUS for a research scholarship award as well as to the National Science and Technology Board of Singapore for a top-up supplement.

Supporting Information Available: Text giving the details of X-ray structural analyses and tables of crystallographic data, refined atomic coordinates and isotropic thermal parameters, anisotropic thermal parameters, and bond lengths and angles for **3a**, **5a**, **5b**, and **6a**. This material is available free of charge via the Internet at http://pubs.acs.org.

OM990569C